COMPUTATION OF NONLINEAR FIELDS AND ORBIT AND SPIN TRANSFER MAPS OF ELECTROSTATIC ELEMENTS USING DIFFERENTIAL ALGEBRAS*

K. Makino†, E. Valetov, M. Berz, Michigan State University, East Lansing, MI 48824, USA

Abstract

Traditionally most large storage rings for nuclear and high energy physics use magnetic elements for focusing and bending. However, recent interest in the study of the possible existence of an electric dipole moment (EDM) of protons, deuterons and others requires the use of electrostatic elements in rings, and would even greatly benefit from the use of purely electrostatic lattices without any magnetic elements. Indeed the classical Thomas-BMT equation describing the motion of the spin due to a magnetic dipole moment coupling to magnetic fields can be augmented to analogously also describe the effects of a possibly present electric dipole moment coupling to electric fields, and the additional term would lead to detectable effects. We discuss how to address and resolve various problems appearing in the simulation of such lattices. We begin with methods that allow the computation of nonlinear fields of elements, and in particular their fringe fields, using DA-based PDE solvers, and proceed to the computation of high-order transfer maps, typically up to order 7 or 9. We also discuss a problem arising in these rings, especially the possible nonconservation of the particle energies.

THE DA PDE FIELD SOLVER

The electric and magnetic rigidities $\chi_e = pv/q$ and $\chi_m = p/q$ describe the strengths of coupling to the electric and magnetic fields [1]. Due to the additional factor v, the practically achievable bending in electrostatic elements is less than in magnetic elements, which limits their use to moderate energies, and their desired use in storage ring EDM studies [2] represents a new frontier. Beam dynamics simulations of systems containing electrostatic elements encounter various undesirable effects that do not arise in magnet based systems. We start the discussion with a differential algebra (DA) based field solver, which provides an efficient mechanism to compute 3D nonlinear fields while computing a high-order nonlinear transfer map [3].

We outline the principle of the DA PDE solver using a general form of the Laplace equation. We first bring the equation into a fixed point form:

$$V = V|_{y=0} + \int_0^y \frac{1}{b_2}\left[\left(b_2\frac{\partial V}{\partial y}\right)\Big|_{y=0}\right] dy - \int_0^y \frac{1}{b_2}\int_0^y \left(\frac{a_1}{b_1}\frac{\partial}{\partial x}\left(a_2\frac{\partial V}{\partial x}\right)+\frac{c_1}{b_1}\frac{\partial}{\partial z}\left(c_2\frac{\partial V}{\partial z}\right)\right) dy dy,$$

where a_i, b_i, c_i are functions of x, y, z. Viewing it as a DA fixed point problem, we provide the boundary conditions $V|_{y=0}$ and $(b_2 \cdot \partial V/\partial y)|_{y=0}$ as DA quantities, which represents the field description in the midplane, as analytical functions of x and z. The right hand side is contracting with respect to y in the DA framework [3], and we obtain V as a function of x, y, z by calculating the equation in the DA arithmetic iteratively in finitely many steps. The field components can be obtained also by DA arithmetic as the first derivatives of V [3,4].

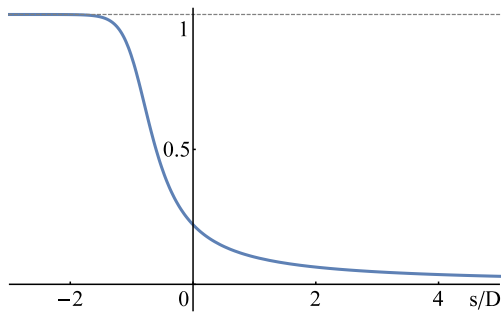

Figure 1: The normalized profile of the fringe field falloff of an electrostatic deflector consisting of two infinitely long capacitor plates, computed by conformal mapping techniques. The effective field boundary is marked by the vertical line. The electric field falls off very slowly on the outside (rightward). s: arclength, $D = 2d$: full aperture.

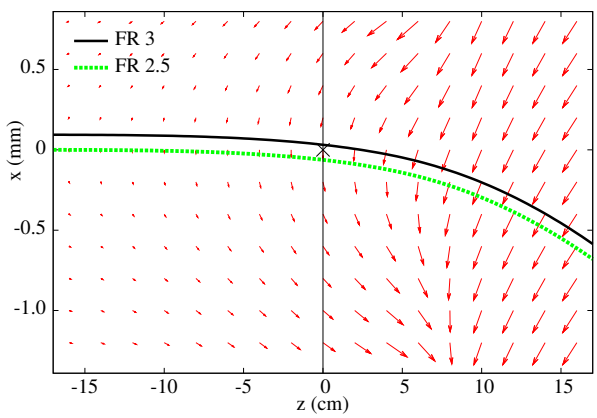

Figure 2: The field distribution in the entrance fringe region of a cylindrical electrostatic deflector; the default falloff, $d = 5$ cm, $R = 24.7$ m, E_z is multiplied by 10^4 for emphasis. The reference trajectories by fringe field modes FR 3 and FR 2.5 are shown. "×" marks the entrance position of the hard edge model (no fringe field).

* Work supported by the U.S. Department of Energy.
† makino@msu.edu

ISBN 978-3-95450-136-6

One carefully attempts to keep the main field of an electromagnetic element constant along the reference trajectory. However in the fringe field region, unavoidable nonlinearity in the motion and hence aberrations are introduced. Figure 1 shows an example fringe field falloff in the midplane along the reference orbit arclength s. The fringe field nonlinearity affects particles at different locations from reference orbit differently due to the curvature of field lines. The DA PDE solver is utilized to obtain the full 3D fringe fields from a suitable analytical function of only s describing the field falloff along the reference orbit in the midplane. The fields of the entire element now can be obtained via the DA PDE solver by supplying the necessary boundary conditions, for example, the DA multiplication of the s-dependent Enge function and the midplane main field. The field shown in Fig. 2 is computed in such a way.

TRANSFER MAP COMPUTATION

Once the fields are known, the equations of motion determine the final status of the coordinate variables $\vec{Z}_f$ depending on the initial status $\vec{Z}_i$. Except for simplified models of electromagnetic elements, one may resort to numerical integration of the differential equations. Using the DA method, one can readily obtain a nonlinear high-order transfer map $\vec{Z}_f = \mathcal{M}(\vec{Z}_i)$ including spin dynamics [3, 5] necessary for the EDM studies. The DA PDE solver is the main mechanism to supply the 3D fields including the derivatives at any position along the transfer map flow integration for nontrivial electromagnetic elements in the code COSY INFINITY [6], and it frees the code from the need to rely on the conventional field computation methods such as FEM and BEM as well as subsequent numerical interpolation and numerical differentiation.

In the hard edge model of the example cylindrical deflector in Fig. 2, the field is zero before the effective field boundary $z = 0$, so the reference trajectory approaches from the left and enters the deflector at $(z, x) = (0, 0)$. However in practice, when considering the unavoidable fringe field, the non-zero field before the boundary already bends the trajectories of the particles. Even the reference trajectory becomes different from the ideal hard edge model; the green dashed curve labeled "FR 2.5" shows the reference trajectory when it approaches from far left at $x = 0$, traveling parallel to the z axis, having quite an offset from $(0, 0)$ due to the influence of the fringe field. This can have far reaching consequences especially in electrostatic elements with their generally slower field falloff, and in particular introduces discrepancies in the resulting transfer maps [7].

The fringe field computation mode FR 2.5 in COSY INFINITY calculates the transfer map along the reference trajectory as described above. This is the easiest way to utilize to treat nonlinear fringe fields, though the reference trajectory throughout the element does not form the expected mirror symmetry about the middle of the element. In order to enforce this symmetry, one can first integrate the reference orbit backwards from the middle of the element, and then shift and rotate the element to account for the resulting deviations. This is done in the mode FR 3, and the resulting reference trajectory in the 22.5° deflector, which has an arc length of ~ 10 m, is shown in the black curve in Fig. 2, resulting in ~ 0.1 mm offset from the FR 2.5 case.

Besides the problem of the trajectory offset, there is another major problem since particle optical elements with fringe fields are usually described by three separate parts, namely the entrance fringe field, the main field, and the exit fringe field. In electrostatic elements, at the end of the entrance fringe fields there are nonzero potentials affecting the particle's energy. If this is followed by a shift or rotation of the reference orbit to line up with the subsequent main field, as is usually done, this leads to a discontinuity

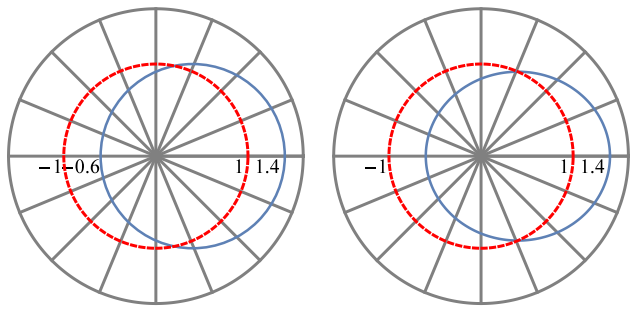

Figure 3: The reference orbit of radius 1 m (dashed red) and an orbit starting at the position displaced rightward by 0.4 m (blue). The system consists of 16 sectors. (left) In the uniform magnets, the displaced orbit is circular with radius 1 m. (right) In the electrostatic spherical deflectors, the displaced orbit is Keplerian elliptic if nonrelativistic.

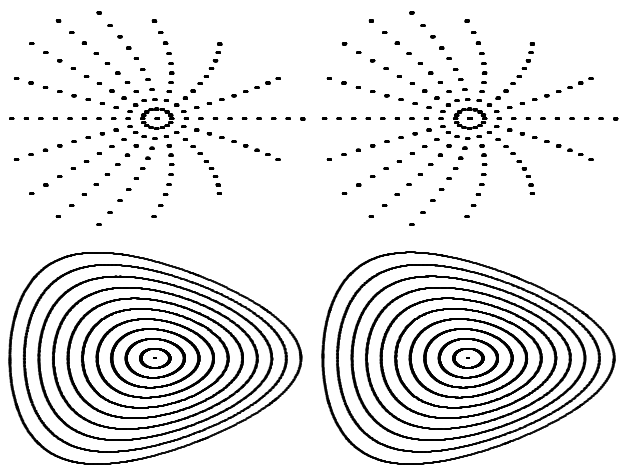

Figure 4: Tracking particles long term through a 22.5° electrostatic spherical deflector around the circular reference orbit with deflection radius 1 m (see Fig. 3) for 160,000 times by (left) pushing through a high-order transfer map, (right) integrating via an 8th order Runge Kutta integrator – this figure and Figs. 5, 6. Particles are launched horizontally up to $x_{\mathrm{ini}} = 0.4$ m, and the x-a phase space motion is shown for nonrelativistic (top) and relativistic (bottom) cases. $|a|$ reaches to 0.46.

ISBN 978-3-95450-136-6

in the potential, and thus a violation of energy conservation. While seemingly small, these effects can very detrimentally build up in repetitive systems. Thus different from common particle optical practice, the discussed fringe field computation modes FR 3 and FR 2.5 carry the computation throughout the entire element including the entrance and exit fringe field regions in a single operation.

A BENCHMARK EXAMPLE

Electrostatic deflectors, while presenting difficulties in particle optical simulations, allow interesting and far-reaching cross checks [6, 7]. Here we study spherical deflectors in detail, where the electrostatic potential is $\propto 1/r$, so the system represents a Kepler problem. In the nonrelativistic case, the motion returns to the exact original state after one full revolution, independent of initial conditions. Thus the transfer map of such a spherical deflector of 360° is an identity map [7].

We perform a challenging long term tracking test based on knowing that the field is radial and nonlinear $\propto 1/r^2$, so the nonrelativistic particles follow Kepler orbits. We pick a circle with radius 1 m as the reference orbit, and consider a system consisting of 16 of 22.5° deflectors as shown in Fig. 3. We study the long term motion of displaced particles up to 0.4 m in the radial direction ($x_{\rm ini}$; Fig. 4) and in the vertical direction ($y_{\rm ini}$; Figs. 5, 6), each having 10 equidistantly displaced particles. We note that a particle with any radial position displacement follows a 1 m radius circle in uniform magnets (left, Fig. 3), and follows a Kepler ellipse in the spherical electrostatic deflectors (right, Fig. 3).

We performed tracking through the electrostatic spherical deflectors for 160,000 iterations, corresponding to a total of 10,000 orbital revolutions, by the transfer map method with and without symplectification [8], and compared the performance with the numerical integrations using a highly accurate 8th order Runge Kutta (RK) integrator with automatic step size control. In case of the $x_{\rm ini}$ test, the majority of the interesting aspects is seen in the x-a phase space plots corresponding to the radial motion. On the other hand, the $y_{\rm ini}$ test shows interesting aspects in both the x-a and the vertical y-b phase spaces. To represent the motion covering the range of this stress test, nonlinear transfer maps of high order are necessary. In Figs. 4, 5, 6 we used maps of order 19, and no visible difference is observed compared to the plots by RK. One tracking run of 160,000 elements required $\sim$ 400 s by RK. The corresponding computation by the transfer map method requires the computation of a high order transfer map for one 22.5° deflector in the beginning, and the remaining task is to apply the transfer map repeatedly for 160,000 times. This is very fast using the DA method; the 2D $x_{\rm ini}$ test takes $\sim$ 7 s, while the 4D $y_{\rm ini}$ test takes $\sim$ 140 s. To cross check the results, we also performed the transfer map tracking computations with symplectification [8], where the $x_{\rm ini}$ test takes $\sim$ 40 s and the $y_{\rm ini}$ test takes $\sim$ 950 s, and it results in complete agreement in the resulting plots.

Nonrelativistic particles follow closed Kepler ellipses, so each of 10 displaced particle leaves 16 breadcrumbs at the exactly same 16 phase space positions in every revolution. If the motion were linear, all breadcrumbs would line up straight and symmetrically. However, in reality the motion is very nonlinear, resulting in the curved structure seen in the top plots in Fig. 4. The plots in the $y_{\rm ini}$ test look straightforward at first glance, but a careful inspection reveals the complication due to the 3D elliptic motion. For example, the top plots in Fig. 5 stretch out leftward less than they do on the right. In the relativistic case, the orbits are no longer closed due to precession of perihelion resulting from the relativistic change of mass during the revolution, corresponding to Einstein's precession of the perihelion of Mercury. The bottom plots in Fig. 5 show the effect of this precession, and coupling effect arise in the x-a plots in Fig. 6.

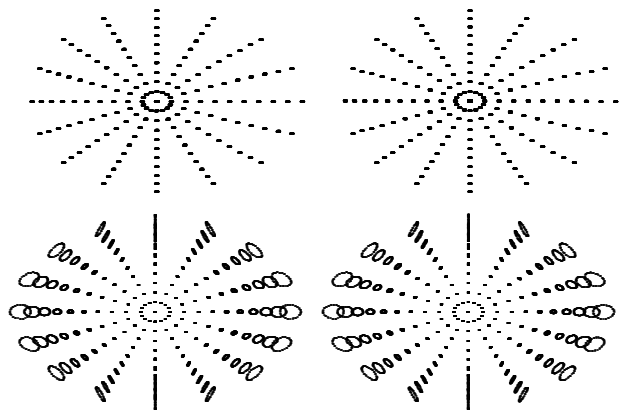

Figure 5: Particles are launched vertically up to $y_{\rm ini} = 0.4$ m. The y-b projection of the motion is shown for nonrelativistic (top) and relativistic (bottom) cases. $|b|$ reaches to 0.43. (left) map, (right) RK.

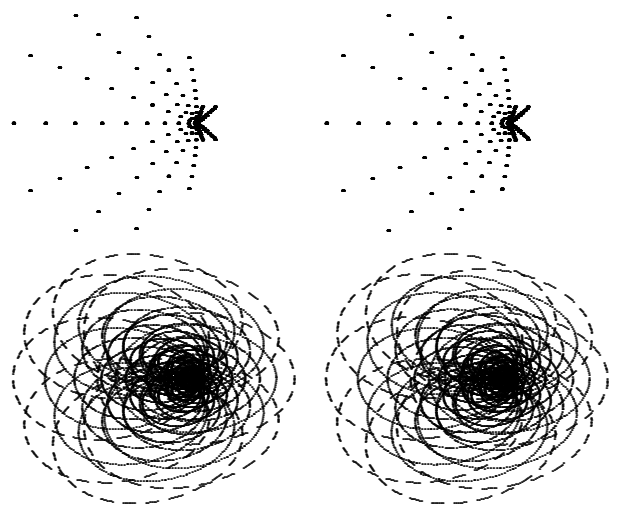

Figure 6: Particles are launched up to $y_{\rm ini} = 0.4$ m as in Fig. 5. The x-a projection of the motion is shown. x and a, initially 0, reach to the range $-0.15 \le x \le 0.02$, $|a| \le 0.13$ (top, nonrelativistic), and $-0.15 \le x \le 0.08$, $|a| \le 0.15$ (bottom, relativistic). (left) map, (right) RK.

ISBN 978-3-95450-136-6

REFERENCES

[1] M. Berz, K. Makino, W. Wan, *An Introduction to Beam Physics*. CRC Press, Taylor & Francis Group, London, Boca Raton (2014).

[2] Storage Ring Electric Dipole Moment Collaboration. http://www.bnl.gov/edm/. JEDI Collaboration (Jülich Electric Dipole Moment Investigations). http://collaborations.fz-juelich.de/ikp/jedi/.

[3] M. Berz, *Modern Map Methods in Particle Beam Physics*. Academic Press, San Diego (1999).

[4] K. Makino, M. Berz, C. Johnstone, "High-order out-of-plane expansion for 3D fields," International Journal of Modern Physics A **26**, 1807 (2011).

[5] M. Berz, K. Makino, "Advanced computational methods for nonlinear spin dynamics," IOP Journal of Physics **295**, 012143 (2011).

[6] M. Berz, K. Makino, "COSY INFINITY version 9.2 beam physics manual," Technical Report MSUHEP-151103, Michigan State University (2015).

[7] K. Makino, M. Berz, "Dynamics in electrostatic rings via high-order transfer maps," Microscopy and Microanalysis **21** Suppl. **4**, 36 (2015).

[8] B. Erdélyi, M. Berz, "Optimal symplectic approximation of HHamiltonian flows," Physical Review Letters **87,**11, 114302 (2001).

ISBN 978-3-95450-136-6